Anal. Chem. **2004,** *76,* 6461−6469

Surface Plasmon Resonance Near-Infrared Spectroscopy

Akifumi Ikehata, Tamitake Itoh, and Yukihiro Ozaki*

Department of Chemistry and Research Center for Near Infrared Spectroscopy, School of Science and Technology, Kwansei Gakuin University, 2-1 Gakuen, Sanda 669-1337, Japan

Near-infrared (NIR) spectroscopy is ill-suited to microanalysis because of its low absorptivity. We have developed a highly sensitive detection method for NIR spectroscopy based on absorption-sensitive surface plasmon resonance (SPR). The newly named SPR−NIR spectroscopy, which may open the way for NIR spectroscopy in microanalysis and surface science, is realized by an attachment of the Kretschmann configuration equipped with a mechanism for fine angular adjustment of incident light. The angular sweep of incident light enables us to make a tuning of a SPR peak for an absorption band of sample medium. From the dependences of wavelength, incident angle, and thickness of a gold film on the intensity of the SPR peak, it has been found that the absorbance can be enhanced by ∼100 times compared with the absorbance obtained without the gold film under optimum conditions. This article reports the details of the experimental setup and the characteristics of absorption-sensitive SPR in the NIR region, together with some experimental results obtained by using it.

Most of absorption bands in the near-infrared (NIR) region (800−2500 nm) are due to overtones and combinations of fundamental vibrations. They would arise from forbidden transitions if a molecule were an ideal harmonic oscillator. Since O−H, N−H, and C−H bonds have large anharmonic constants, the overtones and combinations of X−H vibrations appear relatively strongly in the NIR region. However, the absorption bands due to the overtones and combination modes are much weaker than those due to the fundamentals in the mid-IR region. The weak absorption in the NIR region allows in situ spectral measurements of a huge variety of materials, and nowadays, NIR spectroscopy has acquired great importance in many areas, e.g., agriculture, foods, pharmacy, polymers, textiles, biotechnology, and medicine.[1−3] In NIR spectroscopy, chemometrics has paved an alternative way to quantitative analysis for subtle changes in spectra.[1,3,4] However, if we cannot get adequate absorption intensity, even chemometrics may not be able to exercise its power. This kind of problem often occurs in the case of microanalysis. According to Lambert−Beer law, a sample with low absorption needs a long path length or a high concentration to achieve adequate signal intensity. In other words, generally speaking the NIR region requires a large quantity of sample. This low absorptivity should be overcome by an experimental approach. Recently, we developed a method for highly sensitive detection of NIR spectra based on surface plasmon resonance (SPR) as a countermeasure against a small amount of sample.[5] This method is newly named "SPR−NIR spectroscopy". SPR−NIR spectroscopy can dramatically cut a working sample volume down to the nanoliter range required for NIR spectral measurements. NIR spectroscopy has traditionally been weak in microanalysis and surface analysis; however, SPR−NIR spectroscopy will make these analyses feasible with enormous absorption enhancement.

SPR is a quantum optical−electrical phenomenon arising from the interaction of light with the oscillation of free electrons that propagates along with the surface bound to a dielectric medium i.e., surface plasmon (SP).[6,7] We cannot think about SPR without the recent rapid development of SPR sensors. The SPR sensors show high performance for the sensitive detection of a minor change in the refractive index of a dielectric sample. However, it is almost impossible to identify the sample by use of the conventional SPR sensors, because they can detect only a change in the refractive index.

We employed a Kretschmann configuration[8] for the SPR−NIR measurement system. The Kretschmann configuration we used is the same as that for attenuated total reflection (ATR), but it has a thin metal film on the reflective surface of an internal reflection element (IRE). Almost all of the SPR sensors adopt this configuration. However, our goal is not sensitive detection of the refractive index but highly sensitive measurement of absorbance. An introduction of a complex refractive index, $\tilde{n}$, leads us to the goal.

$$\tilde{n} = n + i\kappa \tag{1}$$

n and κ represent a real part of the refractive index and an

* Corresponding author. E-mail: ozaki@ksc.kwansei.ac.jp.

(1) Siesler, H. W., Ozaki, Y., Kawata, S., Heise, H. M., Eds. *Near-Infrared Spectroscopy, Principles, Instruments, Applications*; Wiley-VCH Verlag GmbH: Weinheim, 2002.
(2) Raghavachari, R., Ed. *Near-Infrared Applications in Biotechnology*; Marcel Dekker: New York, 2001.
(3) Burns, D. A.; Ciurczak, E. W. *Handbook of Near-Infrared Analysis*, 2nd ed.; Marcell Dekker: New York. 2004.
(4) Næs, T.; Isaksson, T.; Fearn, T.; Davies T. *A User-Friendly Guide to Multivariate Calibration and Classification*; NIR Publications: Chichester: 2002.
(5) Ikehata, A.; Itoh, T.; Li, X.; Jiang, J.; Ozaki, Y. *Appl. Phys. Lett.* **2003**, *83*, 2232−2234.
(6) Kittel, C. *Introduction to Solid State Physics*, 7th ed.; Wiley: New York, 1996.
(7) Kawata, S., Ed. *Near-Field Optics and Surface Plasmon Polaritons*; Topics in Applied Physics 81; Springer-Verlag: Berlin, 2001.
(8) Kretschmann, E.; Reather, H. *Z. Naturforsch., A* **1968**, *23*, 2135−2136.

10.1021/ac049003a CCC: $27.50
Published on Web 10/02/2004

extinction coefficient, respectively. As we all know, the extinction coefficient κ is proportional to the absorption. The key to achieving the high-sensitivity measurement of absorption lies in the fact that SPR is sensitive to the extinction coefficient as well as the refractive index. Kano and Kawata predicted evident enhancement of absorption by SPR and called it "absorption-sensitive SPR".[9]

In 1978, the possibility of absorption-sensitive SPR in the visible region was experimentally demonstrated by Pockrand.[10] In this decade, several research groups have been working on absorption-sensitive SPR in the background of the development of the conventional SPR sensors. Through photochemical efficiency, absorption-sensitive SPR allows the detection of a low-molecular-weight compound. This property has been applied to ion optode and enzyme sensors.[11−13] Ekgasit et al. have recently encouraged this trend by an experimental application to SP field-enhanced fluorescence spectroscopy.[14,15] These studies on absorption-sensitive SPR have been intended as a developed method of the conventional SPR sensors with a monochromatic light such as a laser.

On the other hand, Kolomenskii et al. and Tao's group succeeded in the high-sensitivity detection of visible spectra of a dye solution by use of SPR.[16−18] The purpose of their studies is enhancement of the absorption spectra. Their approach is more similar to surface electromagnetic wave (SEW) spectroscopy or surface-enhanced infrared absorption (SEIRA) spectroscopy. SEW spectroscopy was comprehensively studied by Bell et al. in the 1970s as a topic of waveguide techniques for mid-IR and far-IR.[19] Since SEW is just a alias of SP, SEW is essentially not different from absorption-sensitive SPR. SEIRA can be construed as a kind of SEW with a ultrathin metal film. The ultrathin metal films used for SEIRA do not have smooth surfaces but consist of metal islands smaller than the wavelength of light. SEIRA has recently received considerable interest from the points of the elucidation of its mechanism and its applications to surface analysis.[20,21] It is interesting to examine the effect of an ultrathin metal film on absorption-sensitive SPR, but we are not concerned with it in this paper.

Although absorption-sensitive SPR (or SEW) has been applied to the visible and mid-IR regions, there has been no previous study focusing on the NIR region. In the previous letter,[5] we reported enormous absorption enhancement of a water band near 5173 cm^{-1} by SPR−NIR. This paper describes the details of the experimental setup and characteristics of absorption-sensitive SPR in the NIR region and some of the experimental results that we obtained by using the instrument developed by ourselves.

THEORY AND CALCULATION

Theory for the conventional SPR is applicable to the calculation of absorption-sensitive SPR. In this paper, we concentrate on dependence of change in absorbance, that is to say, the imaginary part of refractive index.

Refractive Index of Prism. For the calculation, we represent a dispersion relation of a prism-IRE by the Sellmeier equation given by

$$n_p^2 = \alpha + \frac{\beta\lambda^2}{\lambda^2 - \gamma} + \delta\lambda^2 \tag{2}$$

where n_p and λ represent the refractive index of the prism and wavelength (nm), respectively. The parameters, α, β, γ, and δ are determined by a nonlinear least-squares curve fitting to available discrete data of refractive indices corresponding to BK7 and LaSF15N. The data were downloaded from the web page of Sigma Koki Co., Ltd.[22] The best values of the parameters are listed in Supporting Information (Table S1). The standard deviations between eq 2 and the discrete data were less than 0.1. We have an assumption that the prisms have no absorption over the whole range of wavelengths.

Dielectric Constants of Metals. It is essential to choose a metal that has adequate dielectric contact with a sample for SPR. The metal should have a complex dielectric constant, $\tilde{\epsilon}_m$, whose absolute values of a real part, ϵ_1, and an imaginary part, ϵ_2, must be widely different, and ϵ_1 should be negative.

$$\tilde{\epsilon}_m = \epsilon_1 + i\epsilon_2 \tag{3}$$

In practice, gold is an ideal metal for use in SPR. The dielectric constant of gold as a function of wavelength (angular frequency, $\omega = 2\pi/\lambda$) is also required for the calculation. We employed the data obtained by Johnson and Christy as reliable data,[23] and reproduced them by Drude formula as follows.

$$\tilde{\epsilon}_m = \epsilon_\infty - \frac{\omega_p^2}{\omega^2 + i\omega\omega_\tau} \tag{4}$$

The real part, ϵ_1, and the imaginary part, ϵ_2, of eq 3 are represented by

$$\epsilon_1 = \epsilon_\infty - \frac{\omega_p^2}{\omega^2 + \omega_\tau^2} \tag{5}$$

$$\epsilon_2 = \frac{\omega_p^2\omega_\tau}{\omega^3 + \omega\omega_\tau^2} \tag{6}$$

where ω_p and ω_τ are plasma frequency and damping frequency, respectively, and they have the unit of hertz. The constant ϵ_∞

(9) Kano, H.; Kawata, S. *Appl. Opt.* **1994**, *33*, 5166−5170.
(10) Pockrand, I. *Surf. Sci.* **1978**, *72*, 577−588.
(11) Kurihara, K.; Suzuki, K. *Anal. Chem.* **2002**, *74*, 696−701.
(12) Fujii, E.; Koike, T.; Nakamura, K.; Sasaki, S.; Kurihara, K.; Citterio, D.; Iwasaki, Y.; Niwa, O.; Suzuki, K. *Anal. Chem.* **2002**, *74*, 6106−6110.
(13) Kurihara, K.; Nakamura, K.; Hirayama, E.; Suzuki, K. *Anal. Chem.* **2002**, *74*, 6323−6333.
(14) Ekgasit, S.; Thammacharoen, C.; Knoll, W. *Anal. Chem.* **2004**, *76*, 561−568.
(15) Ekgasit, S.; Thammacharoen, C.; Yu, F.; Knoll, W. *Anal. Chem.* **2004**, *76*, 2210−2219.
(16) Kolomenskii, A. A.; Gershon, P. D.; Schuessler, H. A. *Appl. Opt.* **2000**, *39*, 3314−3320.
(17) Boussaad, S.; Pean, J.; Tao, N. J. *Anal. Chem.* **2000**, *72*, 222−226.
(18) Wang, S.; Boussaad, S.; Tao, N. J. *Rev. Sci. Instrum.* **2001**, *72*, 3055−3060.
(19) Bell, R. J.; Alexander Jr. R. W.; Ward, C. A.; Tyler, I. L. *Surf. Sci.* **1975**, *48*, 253−287.
(20) Hartstein, A.; Kirtley, J. R.; Tsang, J. C. *Phys. Rev. Lett.* **1980**, *45*, 201−204.
(21) Osawa, M.; Ataka, K.; Yoshii, K.; Nishikawa, Y. *Appl. Spectrosc.* **1993**, *47*, 1497−1502.
(22) http://www.sigma-koki.com/.
(23) Johnson, P. B.; Christy, R. W. *Phys. Rev. B* **1972**, *6*, 4370−4379.

denotes dielectric constant in the high limiting frequency. Especially in the NIR region the experimental results by Johnson and Christy are quite well reproduced by the Drude formula. We calculated the suitable parameters for gold by a nonlinear least-squares curve-fitting method. The best values of parameters are $\omega_p = 1.35 \times 10^{16}$, $\omega_\tau = 1.25 \times 10^{14}$, and $\epsilon_\infty = 8.3835$.

Refractive Index of Sample. To model the behavior of absorption-sensitive SPR, the refractive index of a dielectric sample medium, $\tilde{n}$, must have a complex form, eq 1. Now, the extinction coefficient κ is related to absorbance, A, by the formula

$$\kappa = A\lambda/4\pi l \tag{7}$$

where l denotes an optical path length. For the calculation, κ is calculated from experimental data of absorbance, A, measured by transmission mode. On the other hand, the real part, n, should be originally derived from κ by means of the Kramers−Kronig relation. However, we simply employed an approximate formula of the refractive index of water as a function of wavelength.[24]

Condition of SPR. Dispersion relation of light in the prism is given by

$$k_p = n_p(\omega/c) \tag{8}$$

where k_p denotes a wave vector of the light in the prism. As we all know, c is the velocity of light in a vacuum. The dispersion relation of SP is written by

$$k_m = \frac{\omega}{c} Re\left[\frac{\tilde{\epsilon}_m \tilde{n}_s^{\,2}}{\tilde{\epsilon}_m + \tilde{n}_s^{\,2}}\right]^{1/2} \tag{9}$$

Since the SP is associated with an evanescent field, it can be excited by irradiation with an evanescent light wave satisfying the following condition of the dispersion relation at the boundary between the metal and the sample medium.

$$k_m = n_p(\omega/c)\sin\theta \tag{10}$$

The right-hand side of eq 10 is the wave vector of the evanescent wave—that is, the x-direction component of the incident light in the prism at an incident angle, θ. Substitution of eqs 2 and 9 into eq 10 gives the SPR angle, θ_{spr}, as a function of wavelength (or wavenumber, $\nu = \lambda^{-1}$) as follows.

$$\theta_{spr} = \sin^{-1}\left(Re\left[\frac{\tilde{n}_s}{n_p}\left(1 - \frac{\tilde{n}_s^{\,2}}{n_m^{\,2} + \tilde{n}_{s2}}\right)^{1/2}\right]\right) \tag{11}$$

Fresnel Reflection. For this calculation, we assume a thin metal film with a perfectly planed surface. Therefore, we can refer to Fresnel reflection. The intensity of reflectance is represented as a function of the incident angle, θ, and the thickness of a gold film, d, with amplitude reflectances, r_{ij}, at boundaries between media i and j for light incident from i to j as

$$R(\theta, d) = \left|\frac{r_{pm} + r_{ms}\exp(2ik_{mz}d)}{1 + r_{pm}r_{ms}\exp(2ik_{mz}d)}\right|^2 \tag{12}$$

Amplitude reflectances r_{ij} of each boundary are written as

$$r_{pm} = \frac{k_{pz}\epsilon_m - k_{mz}\epsilon_p}{k_{pz}\epsilon_m + k_{mz}\epsilon_p} \tag{13}$$

$$r_{ms} = \frac{k_{mz}\epsilon_s - k_{sz}\epsilon_m}{k_{mz}\epsilon_s + k_{sz}\epsilon_m} \tag{14}$$

where suffixes, s, p, and m denote sample, prism and metal, respectively, and k_{pz}, k_{mz}, and k_{sz} indicate z component (parallel to the surface) of wave vectors of incident light inside the prism, metal, and sample, respectively. They are given by

$$k_{pz} = (\epsilon_p(\omega^2/c^2) - k_{px}^{\,2})^{1/2} \tag{15}$$

$$k_{mz} = (\epsilon_m(\omega^2/c^2) - k_{px}^{\,2})^{1/2} \tag{16}$$

$$k_{sz} = (\epsilon_s(\omega^2/c^2) - k_{px}^{\,2})^{1/2} \tag{17}$$

Total Absorbance. The amplitude reflectance r_{ij} is defined for each polarizing direction, namely, $r_{ij\perp}$ for p-polarized light and $r_{ij\parallel}$ for s-polarized light. The reflectance for p-polarized light, $R_\perp$, and that for s-polarized light, $R_\parallel$, are defined by eq 12 with $r_{ij\perp}$ and $r_{ij\parallel}$, respectively. $R_\perp$ and $R_\parallel$ can be written by the intensity of the input light, I^{in}, and that of the output light, I^{out}, as follows.

$$R_\perp = I_\perp^{\,out}/I_\perp^{\,in} \tag{18}$$

$$R_\parallel = I_\parallel^{\,out}/I_\parallel^{\,in} \tag{19}$$

Since the s-polarized light is totally reflected, $R_\parallel$ must be 1. For depolarized incident light, we have the following relation,

$$I_\perp^{in} = I_\parallel^{in} \tag{20}$$

Accordingly, the observable absorbance is denoted by

$$A_E(\nu,\theta, d) = -\log R_\perp = -\log(I_\perp^{out}/I_\parallel^{out}) \tag{21}$$

EXPERIMENTAL SECTION

The major characteristics of our SPR−NIR instrument are as follows: (i) Fiber optics can be used for remote sensing applications. (ii) One can measure SPR spectra (dependence of wavelength). (iii) One can also measure SPR curves (dependence of incident angle).

Let us describe the system in more detail.

Instrumental Setup for SPR Measurement. Figure 1a shows the experimental setup that we have developed. It consists of a homemade SPR accessory with the Kretschmann configuration, a FT-NIR spectrometer (VECTOR22/N, Bruker Optics)

(24) Thormahlen, I.; Straub, J.; Grigull, U. *J. Phys. Chem. Ref. Data* **1985**, *14*, 933−945.

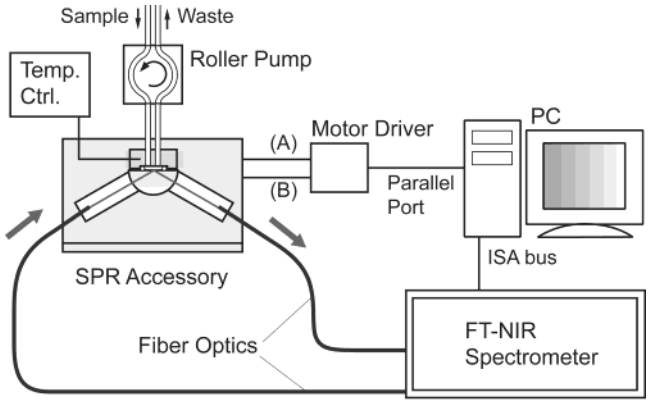

(a) Schematic of the SPR-NIR Instrument

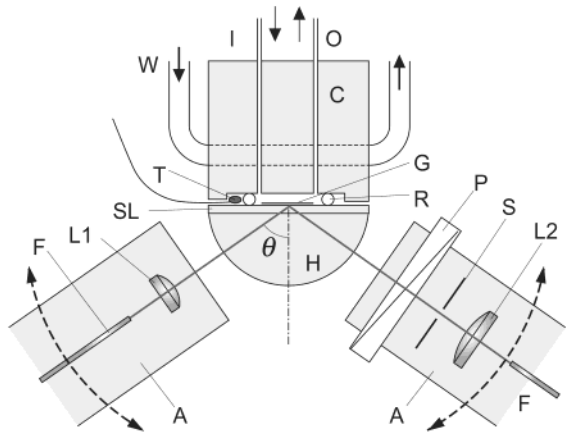

(b) Optical Layout of SPR Attachment

Figure 1. (a) Schematic diagram of the SPR−NIR setup. (b) Optical layout of the SPR attachment of the Kretschmann configuration. The components used are as follows: (F) quartz fiber optic; (L1,L2) plano-convex lens; (H) hemicylinder prism; (SL) slide glass; (P) polarizer; (S) slit; (C) flow cell block; (I) inlet tube; (O) outlet tube; (R) O-ring; (G) gold film; (W) water circulation; (A) angle adjustment arm; (T) bead thermistor.

equipped with an InGaAs photodiode, fiber optics, and a personal computer. The incident white light beam from the external port of the FT-NIR spectrometer is sent through a quartz fiber optic (F) (the low-OH silica/silica clad, 0.6-mm diameter) to the homemade SPR accessory. The detail of the SPR accessory is illustrated in Figure 1b. The light is collimated at the end of the fiber optic with a 4.0-mm focal length, plano-convex lens (L1) (SLM-04-04P, Sigma Koki Ltd., Tokyo, Japan) and a 20-mm-i.d. hemicylinder prism (H). We prepared two kinds of hemicylinder prisms made of two kinds of glasses—BK7 (n_D = 1.517) and LaSF15N (n_D = 1.87). The collimated incident beam, whose beam width is ~2 mm in the hemicylinder prism, is internally reflected on the top surface. The reflected beam passes through a polarizer (P) (SPFN-30C-26, Sigma Koki Ltd.) and a slit (S) (slit width 200 μm) to decrease the effect of the angular dispersion of the prism. It is then focused into another fiber optic with a plano-convex lens (L2) (10-mm focal length, SLSQ-08-10P, Sigma Koki) to send it back to the FT-NIR spectrometer.

Sample liquid was infused into a temperature-controlled flow cell (C) from its inlet (I), and the used liquid is flashed out to the outlet tube (O). The inner wall of the flow cell is coated with Teflon to resist chemicals. To keep the temperature of the sample at 25 °C, water was circulated (W) through the flow cell block with a bead thermistor (T). To fill this flow cell, at least 1 mL of liquid sample is required. However, taking account of a penetration depth of the evanescent wave (~1 μm in depth), we can reduce the working sample volume down to 10 nL or less.

The tips of the fiber (SMA connectors), the collimation lenses, the slit, and the polarizer are mounted on angle adjustment arms (A), allowing us to vary the incident angle, θ from 40° to 90°. The variation of the incident angle is realized by means of a precision positioning stage (SGSP-20-85, Sigma Koki Ltd.) with a motor driver (SG-154MSC, Sigma Koki Ltd.). This stage pushes the angle adjustment arms up with a minimum step size of 0.000 04°.

Rotation of the polarizer by 90° permits us to measure both background spectra and sample spectra without removal of the sample. The background spectra, $I_{\parallel}^{out}(\nu)$ and the sample spectra, $I_{\perp}^{out}(\nu)$ can be measured with *s*-polarized light and *p*-polarized light, respectively. Finally, absorption spectra−SPR spectra are given by eq 21. A small two-phase stepper motor with a gear pair rotates the polarizer.

Data Acquisition Process. For the system control and data acquisition, we wrote a program and compiled it in Delphi 6 (Borland Software Corp.). To rotate the stepper motors for the polarizer and the incident angle adjustment arms, rectangular pulses generated by the homemade program are sent from the parallel port of the PC. This program can also execute a spectral acquisition command on OPUS-NT software (Bruker) with DDE communication at the right time. The SPR spectra were measured at a 2-cm^{-1} resolution, and eight scans were coadded. The flowchart of the data acquisition process is shown in Supporting Information (Figure S1).

Preparation of Substrate. For handiness, a glass slide (thickness 1 mm) with a thin gold film was placed on the prism with suitable index matching fluid. Poly(ethylene glycol) (M_w = 300, Wako Pure Chemical, Osaka, Japan) and refractive index liquid (Cargill Series H) were used as the matching fluids for BK7 and LaSF15N, respectively.

The gold films were prepared by vacuum deposition. A thin gold wire (purity: 99.95%, diameter 0.25 mm) was purchased from Niraco Co.(Tokyo, Japan). It was cut to a proper length as a deposition source. The piece of gold was loaded into a tungsten boat. The distance between the source and the glass slide substrates was 10 cm. To make a smooth flat surface, the whole piece of gold was evaporated as quickly at a pressure of 3×10^{-3} Pa. After the deposition, the substrates were further kept inside the vacuum bell jar for 30 min to cool. The thickness of gold films, *d*, on the glass slide was determined by transmittance with the incident light perpendicular to the film by using the same FT-NIR spectrometer. The thickness of the gold films calculated by use of the Fresnel formula considering the multiple reflection is listed in Table 1.

ATR/Transmittance Measurement. For the ATR measurement, a glass slide without a gold film was used. To increase the light intensity, both the background and sample scans were performed without the slit. The incident angle was fixed at 69.0° for the BK7 prism and 51.0° for the LaSF15 prism. For comparison, transmittance spectra were also measured with a 0.3-mm path

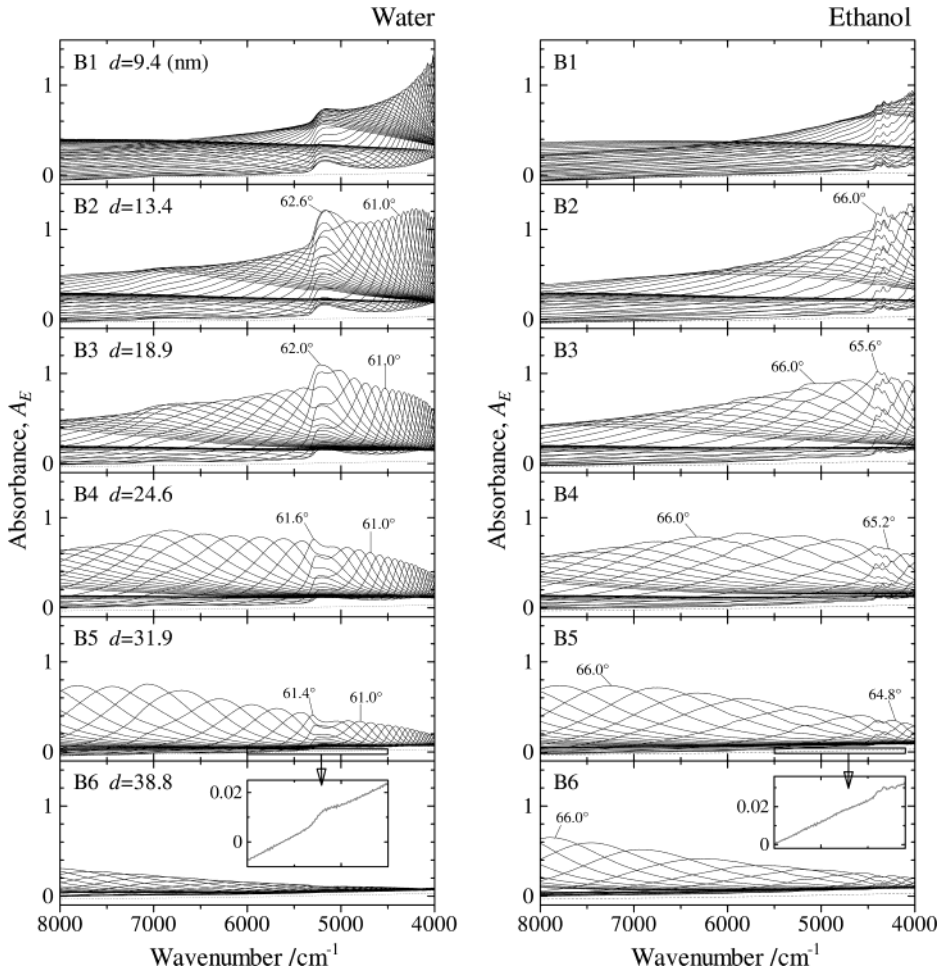

Figure 2. SPR−NIR spectra in the 8000−4000-cm^{-1} region of water and ethanol on gold films with different thicknesses (B1−B6) on the BK7 prism. The spectra were measured over an incident angle range of 57.5°−65.5° for water and of 62.0°−68.0° for ethanol. The data are shown with an increment of 0.2°. The dashed lines represent ATR spectra measured at $\theta = 69.0°$. The insets show enlarged ATR spectra (the 6000−4500-cm^{-1} region for water and the 5500−4100-cm^{-1} region for ethanol).

Table 1. Thickness of Gold Films (nm) on BK7 (B1−B6) and LaSF15 (L1−L5)

code	1	2	3	4	5	6
BK7(B)	9.4	13.4	18.9	24.6	31.9	38.8
LaSF15(L)	12.9	14.7	20.4	27.0	35.7	

length quartz cell by use of the same FT-NIR spectrometer. Throughout all of the experiemnts (SPR−NIR, ATR, transmittance), doubly distilled water and pure ethanol (infinity pure grade, Wako Pure Chemical Industries Ltd.) were used.

RESULTS AND DISCUSSION

SPR−NIR Spectra. Figure 2 shows SPR−NIR spectra of water (left panels) and ethanol (right panels) in the 8000−4000-cm^{-1} region for the six gold films with different thicknesses (B1−B6) on the BK7 prism. The spectra were measured over an angular range of 57.5°−65.5° for water and of 62.0°−68.0° for ethanol with an increment of 0.05°. For easiness in seeing the figures, only the spectra measured at an increment of 0.2° are shown in Figure 2. The SPR peaks are broadened and shift to higher wavenumbers with the increment in the incident angle.[25]

In each figure, a conventional ATR spectrum measured at $\theta = 69.0°$ is shown (dashed line). The insets in the bottom figures are enlarged ATR spectra in the 6000−4500-cm^{-1} region. The inset spectrum of water (the bottom figure of the left panel) shows an absorption band at 5173 cm^{-1} assigned to the combination of bending and antisymmetric stretching modes of the water molecule.[1] In the inset of ethanol, several combination bands can be observed around 4300 cm^{-1}. In both cases, absorbances of these peaks are less than 0.01. The cause of upward trends of the ATR spectra is an inherent difference in the reflection intensity between *p*-polarized light, $I_{\perp}^{out}$, and *s*-polarized light, $I_{||}^{out}$. Thus, the SPR−NIR spectra also contain this trend. We, however, do not apply any baseline correction to these spectra, because the spectra measured with the same gold film can be directly comparable.

In all the cases in Figure 2, the absorption of the samples in the SPR−NIR spectra is evidently enhanced by SPR compared with that in the ATR spectra, especially when an absorption peak and a SPR peak overlap with each other. The B2 and B3 gold films achieve almost 100-fold enhancement of the absorption bands of water and ethanol compared to the absorbance in the ATR

(25) Frutos, A. G.; Weibel, S. C.; Corn, R. M. *Anal. Chem.* **1999**, *71*, 3935−3940.

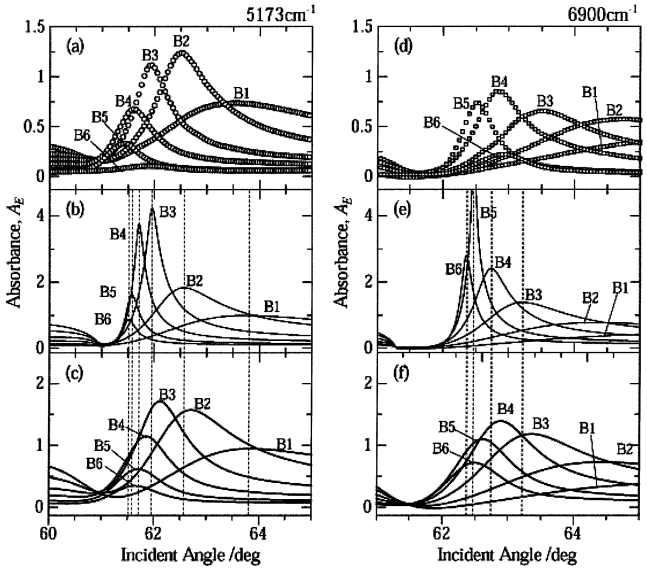

Figure 3. SPR curves at 5173 and 6900 cm^{-1} of water on the BK7 prism for each gold film as a function of incident angle, θ. (a, d) experimental results; (b, e) calculated results by eq 21; (d, f) calculated results by convolution with a Gaussian distribution function with a fwhm of 0.5°.

spectra. Furthermore, note that envelope curves of top ridges of the SPR−NIR spectra of water convex upward in the cases of B1−B3, whereas they concave downward in the cases of B4−B6 in the water combination band region, depending on the thickness of gold films. Enhancement of the overtone band of water around 6900 cm^{-1} can also be observed by the convex curve especially for B3 and B4. For the SPR−NIR spectra of ethanol, the envelope curves of B1−B4 convex upward, while those of B5 and B6 concave downward around 4300 cm^{-1}. On the other hand, for the LaSF15 prism, all of the envelope curves of the SPR−NIR spectra convex upward with gold films in the thickness range of 12.9−35.7 nm. The absorbance of SPR peaks is wholly smaller than that for BK7. This is attributed to the fact that the path length of the evanescent wave that is a Goos−Hänchen shift is shortened by the increment of incident angle. The SPR−NIR spectra of water and ethanol by use of the LaSF15 prism are shown in Supporting Information (Figure S2).

Figure 3 compares the SPR absorption at 5173 and 6900 cm^{-1} (water band) calculated by use of eq 21 with the experimental results for each gold film; the open symbols in Figure 3a and d show the experimental results as a function of the incident angle, while the solid lines in Figure 3b, c, e, and f denote the calculated results from the experimental data in Figure 3a and d. The following results were obtained.

(i) The SPR peak angle, θ_{spr}, shifts to a smaller angle with the increase in the thickness of gold film. However, according to eq 10, the condition for SPR does not depend on the thickness of a metal film. This discrepancy between the experiment and theory is thought to be attributed to the absorption of the sample medium. The SPR peaks in Figure 3 were collected at the wavenumbers of the absorption bands of water. This phenomenon is the foundation of the absorption-sensitive SPR technique, and our results are in good agreement with the results reported for the visible region.[11,14]

(ii) The intensity of a SPR peak has a maximum value against the thickness of the gold film. The maximum intensities can be observed by use of the gold film with the thickness of ∼14 nm for 5173 cm^{-1} and ∼25 nm for 6900 cm^{-1}. What has to be noted is the fact that this maximum is not the maximum of absorption enhancement but the maximum of SPR peak height as described later.

(iii) The optimum conditions of the incident angle and the thickness of a gold film for the maximum SPR peak height change with observed wavenumber.

The calculated SPR curves by eq 21 are shown in Figure 3b and e. The Fresnel reflection indicates that calculated SPR peaks should basically be narrower and stronger than those observed by experiment. It is considered that the discrepancy between the observed and calculated SPR curves is due to the dispersion of the lens and the hemicylinder prism. Assuming that the reflected beam profile has a Gaussian distribution through the calculation, we could confirm the broadening of the SPR peaks. Panels c and f of Figure 3 show calculated results obtained by convolution with a Gaussian distribution function with a full width at half-maximum (fwhm) of 0.5°. Considering the dispersion, SPR peaks become broad and shift to higher angles. It would be better for the SPR angle not to consider the dispersion of the optics. However, it is conceivable that the shift of SPR peak angle, θ_{spr}, is due to the absolute error of measurement. These results with the convolution are thus in much better agreement with the experimental results.

In reference to (i), it is additionally obvious in the calculation that the SPR angle, θ_{spr}, becomes constant with increase in the thickness of the gold film (see Figure 3b, e, c, and f). This is the reason thicker gold films (50−60 nm) are used for the conventional refractive index-sensitive SPR sensors.

Consideration of Figure 3 reveals that when a wavenumber of an absorption band of a sample is known beforehand, a strongly enhanced SPR peak can be measured with an optimum thickness of gold film and an optimum incident angle.

By the convolution with an angular distribution (fwhm = 0.5°), SPR−NIR spectra can be also reproduced qualitatively. The figures of the calculated SPR−NIR spectra are shown in the Supporting Information (Figure S3).

Optimization. It is difficult to estimate experimentally how much the intensity of a SPR peak is modified by the presence of absorption, because it is usually impossible to prepare a reference material that does not have absorption but has the same refractive index as that of the sample. However, such a reference material is readily produced on a computer. Now, we will discuss an enhancement factor of absorbance by means of the Fresnel reflection. The enhancement factor (EF) is to be defined by

$$\mathrm{EF} = (A_{spr}|_{\kappa\neq 0} - A_{spr}|_{\kappa=0})/A_{atr} \qquad (22)$$

where $A_{spr}|_{\kappa\neq 0}$ and $A_{spr}|_{\kappa=0}$ denote an absorbance of SPR−NIR spectra of water and that of the reference sample, which does not have an absorption band. To model the EF, we assume an extinction coefficient, $\kappa = 8.62 \times 10^{-4}$ at 5173 cm^{-1} and $\kappa = 1.56 \times 10^{-4}$ at 6900 cm^{-1} for the sample (water). On the other hand, $\kappa = 0$ is assumed for the reference sample. A_{atr} corresponds to $A_{spr}|_{\kappa\neq 0}$ under the condition, $d = 0$.

Panels a and b of Figure 4 show contour plots of the EF calculated by using eq 22 as a function of thickness of gold film, d, and incident angle, θ, for the combination band at 5173 cm^{-1} and

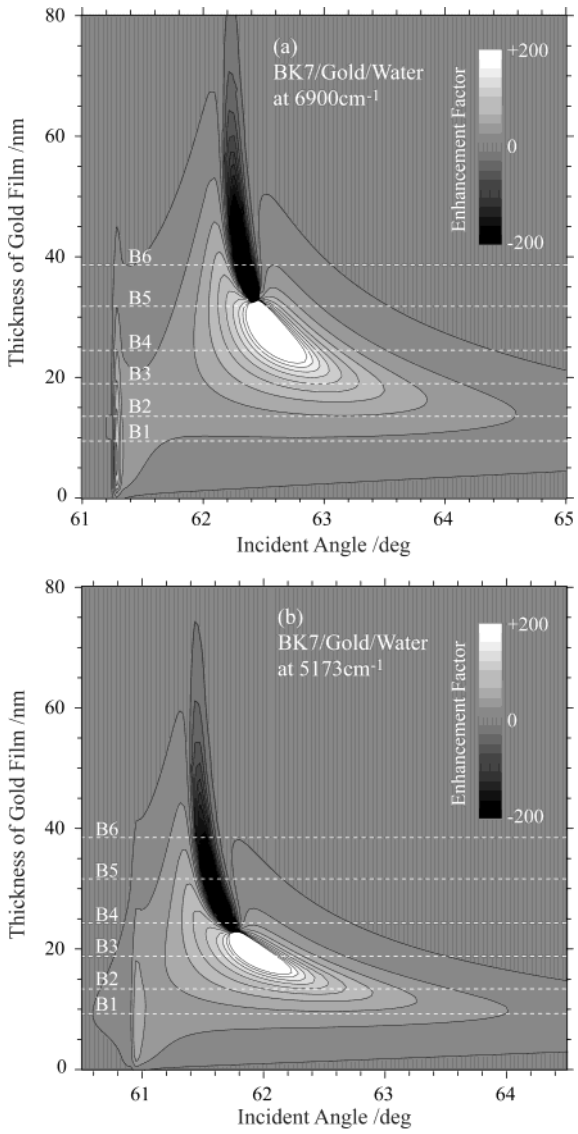

Figure 4. Contour plots of the EF calculated by using eq 22 as a function of thickness of gold film, *d*, and incident angle, θ, for the combination band, 5173 cm^{-1}, (a) and the overtone band, 6900 cm^{-1} (b), of water. The dashed lines indicate the thickness of gold films used for the experiment.

the overtone band at 6900 cm^{-1}, respectively. In this figure, strongly enhanced positive and negative peaks are observed. This result is in agreement with a phenomenon that is specific to absorption-sensitive SPR theoretically predicted in the visible region by Kano and Kawata.[9] The observable signal is due to the light that leaks back from the interface between the metal and the sample. Therefore, if the thickness of a gold film is thinner than the penetration depth of the evanescent wave, the absorption is positively enhanced and vice versa. The maximum efficiency of positive enhancement can be obtained for the combination band (6900 cm^{-1}) and the overtone (5173 cm^{-1}) of water under the conditions given in Table 2.

These contour plots suggest that it can be expected to have enormous enhancement (1000-fold), if one can control the thickness of a gold film with an accuracy of ±0.1 nm, or it can be expected to obtain 100-fold enhancement with an accuracy of our setup. To compare the calculated results with the experimental

Table 2. Calculated Optimum Conditions and EF for the Maximum Efficiency of Positive (+) and Negative (−) Enhancement for the Combination Band (6900 cm^{-1}) and the Overtone Band (5173 cm^{-1}) of Water

ν (cm^{-1})	θ (deg)	d (nm)	EF
6900+	62.44	32.23	12192
6900−	62.42	33.28	−6009
5173+	61.83	21.35	1680
5173−	61.68	25.58	−7333

ones, the thickness of gold films used for the experiment are indicated by dashed lines in Figure 4. We cannot make a simple comparison between the cross section of the EF along the dashed lines and the experimental result of absorbance shown in Figure 3. It is, however, considered that the combination band of water at 5173 cm^{-1} is positively enhanced in the cases of the gold films B1−B3 and negatively enhanced in the cases of B4−B6. These features correspond to the convex and the concave envelope curves of the SPR spectra shown in Figure 2. Thus, our system well demonstrates the essential feature of absorption-sensitive SPR.

Dispersion Curve. The automatic sweep of incident angle and wavenumber of our system enables us to separate SPR−NIR spectra into a dispersion curves and an absorption spectra. Let us discuss the process in detail.

The equation for SPR condition, eq 11, denotes a relation between the SPR peak angle, θ_{spr}, and wavenumber, ν. θ_{spr} is thus observable from Figure 2 as a function of wavenumber, ν. Solving eq 11 for n_s, we have

$$\tilde{n}_s = \sqrt{\frac{n_m^2 n_p^2 \sin^2\theta_{spr}}{n_m^2 - n_p^2 \sin^2\theta_{spr}}} \qquad (23)$$

Substituting experimental data of $\theta_{spr}(\nu)$ into this equation, we can get a dispersion curve—a refractive index of unknown sample, n_s, as a function of wavenumber. Panels a and b of Figure 5 show dispersion curves of water and ethanol, respectively, obtained by use of the experimental data of the SPR peak angle for the BK7 prism. The dashed line in Figure 5a represents a model function of dispersion curve of water at 25 °C.[24]

All of the dispersion curves of the same sample should agree closely with each other. For thick gold films, as stated above, we can look on eq 11 as a function independent of thickness of gold film, *d*. Therefore, the curves for B4−B6 agree fairly well with each other. However, there is considerable disagreement for the thin gold films, B1−B3. If the thickness of a gold film is inadequate for the absorption of the sample, eq 23 should not be used, because it is a model without any regard for the absorption of the sample. For this reason, even the results for B4−B6, deviate from the reference curve of water (dashed line) particularly in the low-wavenumber region. There is thus room for improvement of the model function for the dispersion curve taking into account the effect of absorption.

Absorption Spectra. To extract meaningful information from the SPR−NIR spectra, we will classify the manner of enhancement into two cases as shown in Figure 6. This classification can be a

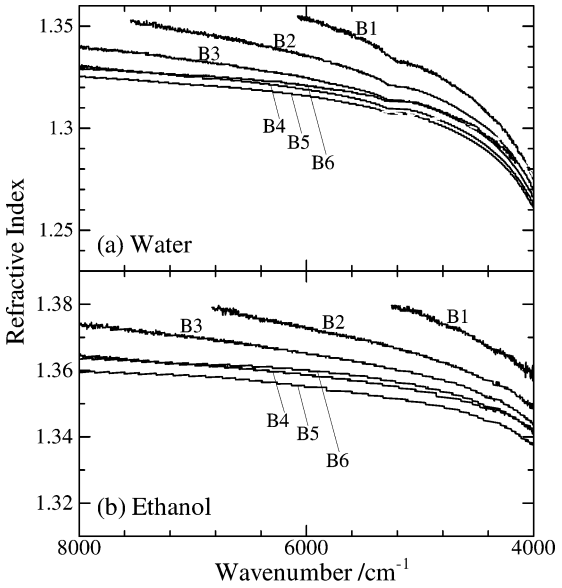

Figure 5. Dispersion curves of water (a) and ethanol (b) converted from the experimental data of the SPR peak angle, θ_{spr}. for BK7 prism by use of eq 23. A dashed line represents a model function of dispersion curve of water at 25 °C.[24]

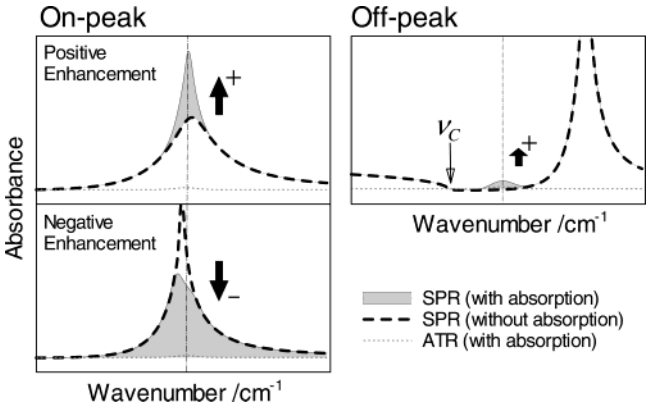

Figure 6. Classification of the absorption enhancement. On-peak condition: The SPR peak right overlaps with the absorption band. Off-peak condition: The absorption band is placed between the SPR peak and a critical wavenumber, ν_c, total reflection occurs. Thick dashed lines and filled area represent SPR spectra of the sample and a reference sample without an absorption band, respectively. An ATR spectrum of this sample is represented by a thin dotted line. The position of an absorption band is indicated with dash−dot lines.

clue to strategies for quantitative analysis of SPR−NIR spectra. Let us assume a dielectric sample medium, which has an absorption band at a wavenumber, indicated with dash−dot lines in Figure 6. An ATR spectrum of this sample is represented by a dotted line. Thick dashed lines and filled area represent SPR spectra of the sample and a reference sample without an absorption band, respectively. When the SPR peak right overlaps with the absorption band, the intensity of the SPR peak is enhanced in a positive or a negative direction depending on the thickness of the gold film (on-peak condition). As Figure 6 indicates, under this condition, a minor change in the absorption of the sample can be readily detected with 1000-fold enhancement.

The absorption band can also be enhanced out of the SPR condition. In other words, an overlap of a SPR peak with an absorption band is not indispensable for enhancement under a

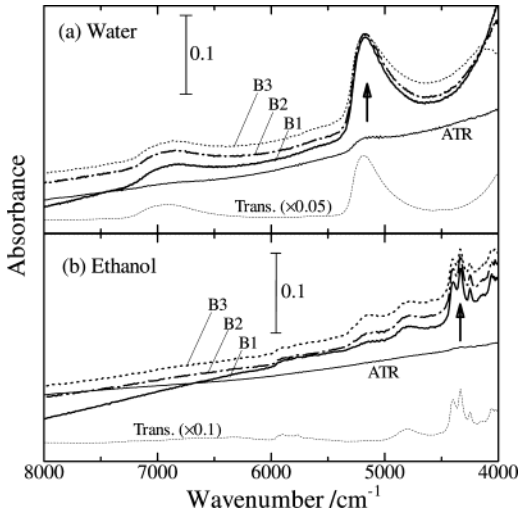

Figure 7. Envelope curves of bottom ridges of the SPR−NIR spectra measured at various incident angles.

total reflection condition. As shown in the right panel of Figure 6, we can obtain 100-fold enhancement, when the absorption band is placed between the SPR peak and a critical wavenumber, ν_c, total reflection occurs (off-peak condition). In this case, the enhanced absorption band is seldom or never deformed. Thus, it can be simply compared with an ATR or transmission spectrum. It is seen from the SPR−NIR spectra of ethanol in Figure 2, particularly for B1 and B2, that the combination bands around 4300 cm^{-1} are enhanced under off-peak condition at low incident angles.

However, a broad band, such as the combination band of water spread out of the wavenumber region of the off-peak condition, and the enhanced band come down to a distorted band compared with the ATR spectrum. An envelope curve of bottom ridges of SPR−NIR spectra measured at various incident angles can be treated as an enhanced spectrum qualitatively comparable to a transmittance spectrum. In Figure 7, envelope curves extracted from the experimental data shown in Figure 2 curves are displayed. ATR and transmittance spectra of water and ethanol are also shown. For the measurement of the transmittance spectra, a 0.3-mm-path length quartz cell was used. It was found that the spectra are enhanced dozens of times compared with the ATR spectra and qualitatively comparable to the transmittance spectra except the trends of their baseline. These trends are due to the imperfect depolarization of the reflection, for the same reason as those for the ATR spectra. The envelope curves of SPR−NIR spectra of ethanol have an absorption peak at 5200 cm^{-1} that is not present in the transmittance spectrum. This peak is due to residual water inside the flow cell. The envelopes may vary slightly for different gold films. If we keep using the same gold film with the flow cell for sample changes, the envelopes will be able to be compared with each other in quantity.

CONCLUSIONS

We have developed a system for the spectral measurement of SPR in the NIR region. The SPR attachment of the Kretschmann configuration can vary an incident angle step by step with a

minimum step size of 0.000 04°. The angular sweep of incident light enables us to make a tuning of a SPR peak for an absorption band of sample medium. The findings of the dependences of wavelength, incident angle, and thickness of a gold film on an SPR curve represent the optimum path to two types of applications. The on-peak condition is well-suited to an application as an absorption-sensitive SPR sensor with either a fixed wavenumber or a fixed angle or both. On the other hand, an enhanced NIR absorption spectrum can be obtained by a sequential angular sweep under the off-peak condition. In both cases, absorbance of any kind of samples is enhanced over 100 times compared with that in an ATR spectrum. Among a variety of optical evanescent wave techniques, our method may be widely used as a quantitative analytical method in a variety of research fields such as surface science, nanotechnology, material science, and life science.

ACKNOWLEDGMENT

This project was supported by a Grant-in-Aid for Young Scientists (B) (15750071) from the Ministry of Education, Culture, Sports, Science and Technology (MEXT).

SUPPORTING INFORMATION AVAILABLE

(Table S1) Coefficients of Sellmeier equation (2) for BK7 and LaSF15N; (Figure S1) Process flowchart of the spectral acquisition; (Figure S2) SPR−NIR spectra of water and ethanol on the LaSF15 prism; (Figure S3) calculated SPR−NIR spectra of water for BK7 and LaSF15. This material is available free of charge via the Internet at http://pubs.acs.org.

Received for review July 7, 2004. Accepted Augest 16, 2004.

AC049003A